ELSEVIER

Materials Science and Engineering A303 (2001) 37–45

MATERIALS SCIENCE & ENGINEERING A

www.elsevier.com/locate/msea

Bi-continuous metal matrix composites

H.X. Peng [a], Z. Fan [a], J.R.G. Evans [b,*]

[a] *Department of Materials Engineering, Brunel University, Uxbridge, Middlesex, UB8 3PH, UK*
[b] *Department of Materials, Queen Mary and Westfield College, University of London, Mile End Road, London E1 4NS, UK*

Received 6 April 2000; received in revised form 27 October 2000

Abstract

Bi-continuous alumina/aluminium composites were made by infiltrating an alumina preform which had the structure of a reticulated ceramic foam. The low density preforms were prepared from a polyurethane suspension of alumina powder which was pyrolysed and sintered after foaming. Higher density preforms consisted of ceramic foams with open cells. All these preforms were infiltrated with 6061 aluminium alloy using a modified squeeze caster fitted with a vacuum system and fine control of speed and pressure. The microstructure of the preform fitted an established relationship between the ratio of window diameter to cell diameter (k) and void volume fraction (V_p). Low k foams were infiltrated fully but on cooling below the solidus, interfacial debonding took place due to differential thermal contraction. This was overcome by modifying the processing conditions. High k foams which had high fractional porosity, retained sound interfacial bonding. The composites possess higher elastic modulus than conventional MMCs with a homogeneous reinforcement distribution at a given volume fraction. The loss of electrical conductivity is negligible in the lower volume fraction range because of the three dimensionally continuous aluminium phase. The experimental results are compared with a number of theoretical predictions.

Keywords: Bicontinuous composite; Alumina; Metal matrix composites (MMCs)

1. Introduction

In recent years, there has been renewed interest in composites with interpenetrating networks including metal matrix composites (MMCs) [1]. Using Newnham's taxonomy which is based on phase connectivity, such materials are designated 3–3 composites since both phases have connectivity in three dimensions [2]. The development of interpenetrating network composites is thus a logical step in the evolution of such materials that began with the fabrication of particulate (0–3) composites. There are some promising advantages resulting from the interconnectivity of phases. For applications where two distinct properties, such as strength and electrical conductivity need to be combined in the same material, they may be ideal.

The realization of other synergistic properties that depend on the interconnectivity of phases requires preparation techniques that allow a wide range of composites to be investigated systematically. The ability to design and fabricate these three-dimensional microstructures raises the possibility of developing materials with multifunctional characteristics: each phase contributing its own properties to the macroscopic properties of the composite. The development of these materials also offers opportunities for testing the theoretical understanding of composite materials in terms of the volume fraction and phase connectivity dependence of transport properties.

In this context, a theoretical model based on a microstructural approach has been devised which allows a range of mechanical and physical properties to be predicted from volume fraction and phase contiguity [3–5]. This model has been shown to fit a range of published data. One of the predictive outcomes of this model is that the mechanical and physical properties depend more directly on the continuous volume fraction of reinforcement than on the overall volume fraction. The model therefore suggests that an interpenetrating network of free matrix and ceramic reinforcement should present an elastic modulus which is higher than that obtained by a random distribution of reinforcement of

* Corresponding author. Tel.: +44-20-78825501; fax: +44-20-89819804.
E-mail address: j.r.g.evans@qmw.ac.uk (J.R.G. Evans).

0921-5093/01/$ - see front matter
PII: S0921-5093(00)01879-7

the same volume fraction. Since the metal matrix is continuous, it should also offer better damage tolerance. The topological optimization of structural elements using finite element analysis also predicts that such arrangements offer the highest stiffness [6]. This coincidence of conclusions from theoretical models provides sufficient justification to explore the property advantages that are expected to accrue from interpenetrating structures in metal matrix composites.

In the literature, most such investigations focus on polymer matrices [7,8] or ceramic matrices [9–12]. The term 'matrix' is ambiguous since both phases in interpenetrating binary composites are three-dimensionally continuous. In the present work, the definition of 'matrix' refers to the phase in the composite having the highest volume fraction. Hence in the published works by Daehn et al. [13] and Prielipp et al. [14] the composites investigated had ceramic volume fractions above 70% and are referred to as ceramic matrix composties. The diverse methods for the fabrication of interpenetrating composites which have appeared in the literature can be classified according to the following approaches: (i) to fabricate a preform with continuous porosity and then to infiltrate it and confer final consolidation [9,10,14]; (ii) to create the composite in situ by a chemical reaction synthesis that leads to an interpenetrating microstructure [13,15–17]. The former is widely applicable to a range of metal, ceramic and polymer systems while the latter is restricted to a limited set of materials.

Although far from new, considerable interest has recently been generated in the fabrication of porous ceramics [18–20]. Apart from their traditional use as refractories or filters, porous ceramics offer an excellent route to the fabrication of interpenetrating composites by the infiltration route. Thus Balch et al. [21] produced a SiC micro-cellular foam from a precursor open-cell polycarbosilane foam that was subsequently converted by oxidative curing and pyrolysis to amorphous or microcrystalline SiC. The foam was infiltrated with 99.9% pure aluminium to make the final composite. The principal difficulty is controllably producing the desired connectivity and spatial distribution of the phases for a given volume fraction, especially on a fine scale. However, recent studies [20,22] of fine ceramic foams prepared from a polyurethane suspension of ceramic particles demonstrate that fine ceramic foam with controlled microstructure can be made.

In the present work, a polymer processing operation is used to prepare a ceramic preform for subsequent infiltration by the metal matrix. A low density fine alumina particle foam was fabricated and, together with some commercially available ceramic foams, employed to make aluminium matrix composites with an interpenetrating microstructure.

2. Experimental details

2.1. Foam preparation

A two-component, polyurethane (PU) foam system (grade ISOFOAM RM6216W) was supplied by Baxenden Chemicals (Accrington, Lancashire, UK) and employed for making ceramic foam. The details have been described elsewhere [20]. The ceramic powder selected was Alcan MA130 alumina with a mean diameter of 4 μm, donated by Alcan Chemicals, Gerrards Cross, UK. The foam fabricated therefrom is designated MA130.

Commercially available alumina foams with nominal relative densities of 10% (POR-AL10), 20% (POR-AL20) and 25% (POR-AL25) were supplied by Hi-Por Ceramics Ltd., Sheffield, UK, and also employed in this study.

The metal used was 6061 aluminium alloy with (0.8–1.2) wt.% Mg and (0.4–0.6) wt.% Si supplied by EMS (Uxbridge, Middlesex, UK). This alloy has liquidus and solidus temperatures of 650 and 582°C, respectively.

2.2. Foam characterization

The densities of the foams were calculated by weighing a regular block and measuring its volume. The microstructures of the ceramic foams were examined using a Jeol JXA840 scanning electron microscope (SEM). The samples with a flat surface were positioned on an aluminium stub using double sided conductive tape: no liquid adhesives or dags were deposited. This allowed window and cell size to be estimated from cells which presented an equator in the fracture surface and from windows by taking the major axis of oblique windows as the true diameter. The cell shape and size together with the window size were examined.

2.3. Composite preparation and microstructural observation

The composites were fabricated by squeeze casting of the 6061 alloy into the ceramic foams. The ceramic foam was placed in the steel die and preheated together with the die to a temperature of $550 \sim 600$°C. The molten aluminium alloy with a temperature of 800°C was then poured onto the preheated ceramic foam. A ram was activated by a 25 tonne hydraulic press (Dassett Engineering Corporation, UK) to force the melt into the foam while evacuation was applied. After the infiltration process a maximum pressure of 65 MPa was maintained until the die cooled and the aluminium phase solidified. The samples were polished and examined using the Jeol JXA840 SEM.

Table 1
Microstructural characteristics of the ceramic foams

	MA130 foam	POR-AL10 foam	POR-AL20 foam	POR-AL25 foam
Relative density (%)	5.9	9.9	16.9	22.4
Window diameter, d (μm)	72	80 ($\pm$16)[a]	58 ($\pm$9)	20 ($\pm$5)
Cell diameter, D (μm)	150 ($\pm$16)	197 ($\pm$30)	215 ($\pm$23)	119 ($\pm$17)
k (d/D)	0.48	0.41	0.27	0.17
Predicted V_p (%)	95.2	91.1	81.9	77.1

[a] Values in parentheses are standard deviation from at least 25 measurements.

2.4. Elastic modulus and electrical resistivity measurement

Due to the existence of the ceramic phase, accurate measurement of modulus is difficult and the use of resonant vibration has proved to be an effective method. In the present work, the measurement of resonant frequencies were performed in flexural mode and a HP 35665A Dynamic Signal Analyzer was employed to detect the fundamental resonance frequencies. The modulus was then deduced by using the EMOD programme for elasticity modulus calculation (J.W. Lemmens INC, USA). Samples with approximate dimensions of 2 mm × 3 mm × 50 mm rested on nodes at about L/4 from each end and were set in vibration by striking with ceramic projectiles. Electrical resistivity measurement was carried out at the National Physical Laboratory by a four point method.

3. Results and discussion

3.1. Microstructural characterisation of the ceramic foams

The measured relative densities of the sintered ceramic foams are shown in Table 1. These values give the ceramic volume fraction in the final metal matrix composite. The microstructure of a partially sintered ceramic foam prepared from polyurethane suspension (MA130) is shown in Fig. 1a at a low magnification. The details of the struts and the particle packing arrangement preserved by partial sintering at 1650°C for 2 h are shown at higher magnification in Fig. 1b. As illustrated before [20], the ceramic foam prepared here possesses porous struts which allow the liquid phase to penetrate not just the foam cells, but the pores in the framework too. The cell size and window size were measured and are given in Table 1.

Fig. 2a and b present the microstructures of the commercial POR-AL20 and POR-AL25 ceramic foams with measured relative densities of 16.9 and 22.4%, respectively, while the POR-AL10 foam with a measured relative density of 9.9% shows a similar structure to the POR-AL20 foam. This series of foams show the steady reduction in window to cell diameter ratio as the ceramic volume fraction increases. Examination of the cell walls shows smooth pore-free sintered surfaces in these commercial foams which contrasts with the partially sintered surfaces of the MA130 foam. As claimed by the supplier, the ceramic foam possesses a uniform distribution of cells and the struts are sintered to full density. As observed in previous studies [20,22], these foams are prepared from finer powders which sinter well.

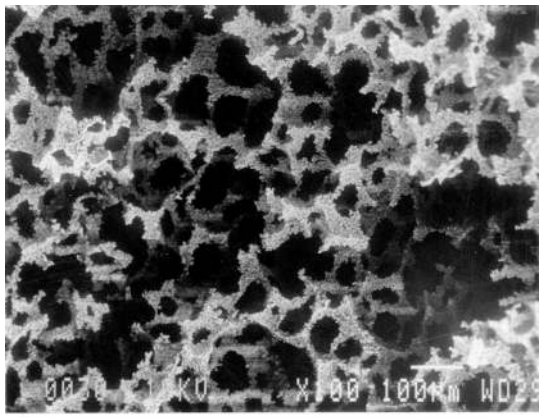

(a)

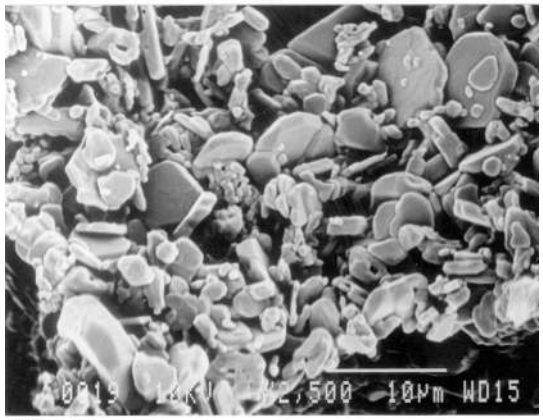

(b)

Fig. 1. The microstructure of sintered ceramic foam prepared from polyurethane suspension (MA130) at a low magnification (a) and higher magnification in (b).

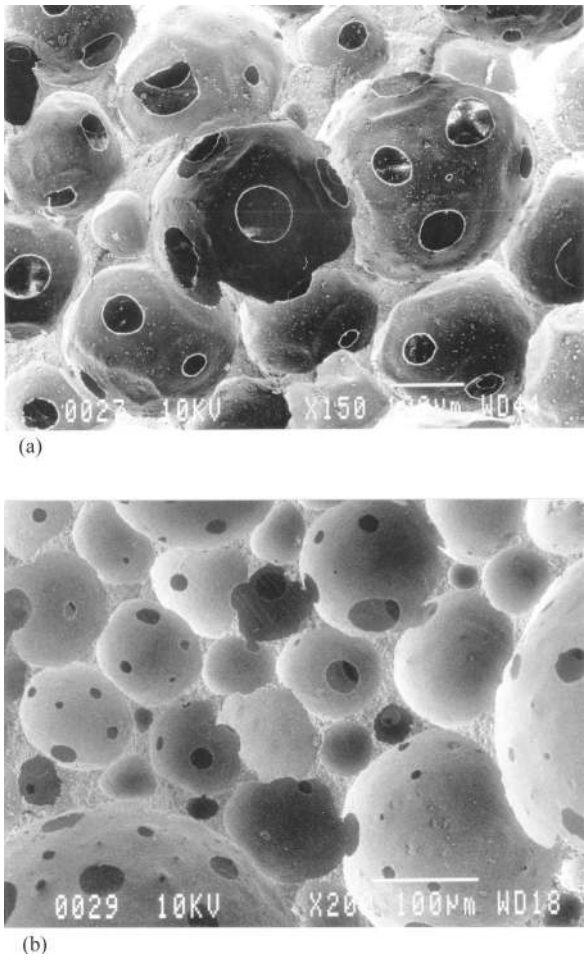

Fig. 2. The microstructure of Hi-POR ceramic foams with measured relative densities of (a) 16.9% and (b) 22.4%.

Comparing Fig. 2a and b, it can be seen that the mean window size decreases and hence the connectivity of the aluminium phase is expected to decrease correspondingly with increasing relative density. For POR-AL25 foam Fig. 2b, the number of windows appears to be less and a few cells tend to be closed. The cell and window sizes were evaluated and the results are listed in Table 1.

Previous studies illustrated that, for cellular ceramics, the degree of reticulation could be expressed in terms of the ratio of window size to cell size k, which can be related to the pore volume fraction, V_p for a pore co-ordination number of 12 [20] by:

$$V_p = \frac{\pi}{\sqrt{2}}\left[\frac{3}{1-k^2} - \frac{5}{3}\left(\frac{1}{\sqrt{1-k^2}}\right)^3 - 1\right]. \quad (1)$$

The calculated value of V_p for each foam is listed in Table 1 from which it can be seen that the value calculated from measured relative density matches the predicted value very well. Based on this relationship, it is not surprising that the POR-AL25 foam which has a measured relative density of 22.4% and a predicted void fraction of 77.1% possesses small windows and that some cells are closed. This foam is close to the critical pore volume fraction in the model array, above which an open cell and below which a closed cell foam is formed, namely $V_p = 0.74$.

As shown in Table 1, the foam with a low relative density possesses a high k and high degree of reticulation. In the present study, the degree of reticulation is of particular importance for three reasons. It is related to the permeability and hence to the pressure gradient generated during melt infiltration. It relates also to the three-dimensional connectivity of the aluminium matrix phase in the composites fabricated therefrom, and hence to a range of transport properties of the composite, such as the electrical conductivity. Furthermore, it is related to the final residual stress state arising from differential thermal contraction. Thus for low k foams, the aluminium matrix has a greater tendency to be in hydrostatic tension after solidification and cooling with consequences for the aluminium/alumina interface.

3.2. The microstructure of the composite

The microstructure of the composite made from the MA130 foam prepared in this work is shown in Fig. 3a and the strut details are given in Fig. 3b at a relatively high magnification. It can be seen that the aluminium phase (dark) has infiltrated the foam well. By using the modified squeeze caster fitted with an evacuating system, the aluminium has infiltrated the open pores of the struts seen in the microstructural examination Fig. 1b. So, the struts themselves are actually an alumina/aluminium composite with a much higher volume fraction of alumina particles than the overall fraction.

In order to determine the volume fraction of the struts and the local volume fraction of the particles in the struts, the polished sample and the SEM photographs were examined using a Q520 Image Analyser (Cambridge Instruments, Cambridge, UK). The results indicated that the volume fraction of alumina particles in the struts is about 50%. This corresponds to a calculated sintered relative density of 58% [22] while the volume fraction of the 'strut' is about 10% of the whole composite which gives an overall particle volume fraction of 5.8%. This agrees with the 5.9 vol.% obtained from the foam characterisation (Table 1).

The microstructures of the composites made by infiltrating the 10 and 17% commercial ceramic foams (POR-AL10 and POR-AL20) are quite different and are shown in Fig. 4a and b, respectively. The dense ceramic does not allow the aluminium to infiltrate but leaves fully dense struts in the composites to form a three-dimensionally continuous phase while the aluminium forms the other. Solidification under high pressure appeared to provide a sound interface between the aluminium phase and the ceramic struts, particularly

for the foam with a high k value Fig. 4a. In this foam, the aluminium phase has greater connectivity than that of the 17% ceramic foam shown in Fig. 4b.

Fig. 5a shows the microstructure of the composite made from the 22% commercial ceramic foam (POR-AL25). In this case, the aluminium does infiltrate the ceramic foam. Obviously, the connectivity of the aluminium phase is the lowest compared with Fig. 4a and b. There is evidence of defects associated with shrinkage and of interfacial debonding. Regarding this issue, Kolhe et al. [23] investigated the residual stress in ceramic matrix composites containing particulate metal and calculated the critical metal particle size for interfacial crack extension. They concluded that, for an Al_2O_3/Ni system, when the particle size of Ni exceeds 3.0 μm, crack extension occurs along the particle/matrix interface upon cooling to room temperature. Within the spherical cells of the composite investigated in this work, high tensile stresses are produced at the interfaces and may cause interfacial debonding. This defect is associated with insufficient compensation for the shrinkage of aluminium during the solidification process

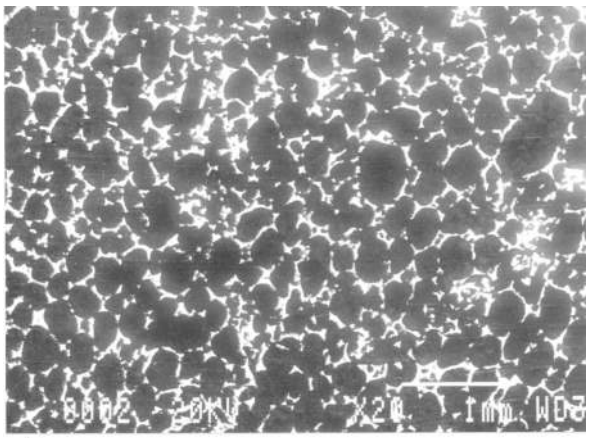

(a)

(b)

Fig. 3. The microstructure of the composite made from the MA130 foam (a) and strut details at high magnification (b).

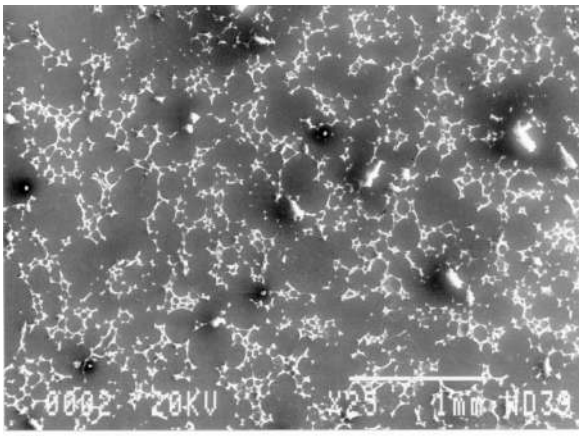

(a)

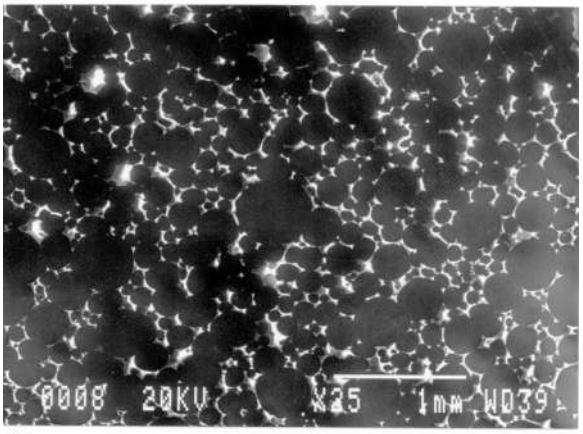

(b)

Fig. 4. A typical scanning electron micrograph of the composite made by infiltrating Hi-POR ceramic foams with relative density (a) 9.9% and (b) 16.9%.

For this reason, the infiltration process was modified and the resulting microstructure of the composite is shown in Fig. 5b while the processing condition is shown in Fig. 6. The pressure (P_{II}) was maintained while the temperature of the die (T_{II}) fell at a cooling rate as low as 0.017°C s^{-1} in the solidification range between the liquidus and solidus of the 6061 alloy. This pressure–temperature schedule contrasts with the original P_I and T_I shown in Fig. 6 and is designed to prolong feeding of the internal architecture of the foam as solidification shrinkage progresses. As shown in Fig. 5b, the microstructure is considerably improved and the defects observed in Fig. 5a were largely eliminated.

The interfacial bonding appears sound as far as can be judged by microscopy as shown in Fig. 5b. In order to characterise the interfacial bond, the fracture surfaces of these samples were examined. Fig. 7a shows the details of the fractured ceramic struts and the aluminium balls which have separated from the ceramic

cell wall in the sample prepared on the initial unmodified schedule. In the centre of the micrograph, the

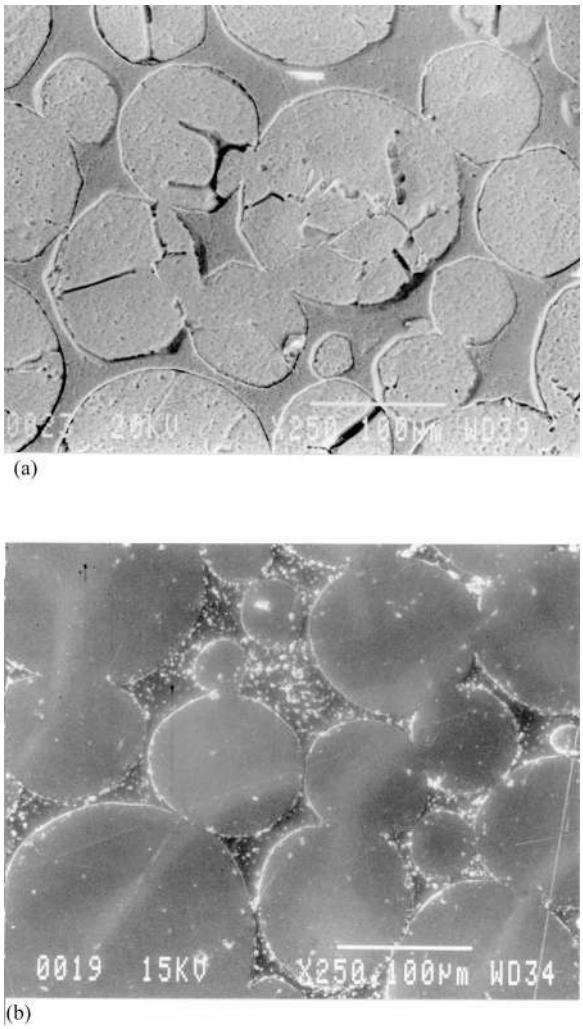

Fig. 5. Scanning electron micrograph of the composite made from POR-AL25 foam under (a) the initial schedule showing signs of shrinkage and interfacial debonding, (b) the modified schedule showing integrity of the structure.

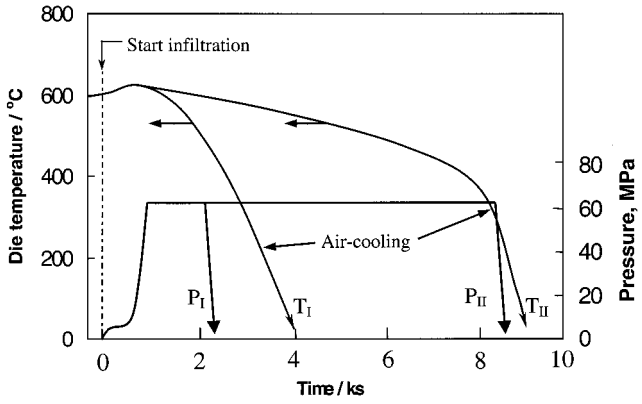

Fig. 6. Processing conditions for preparation of the composites showing (I) initial schedule and (II) the modified schedule for POR-AL25 foam.

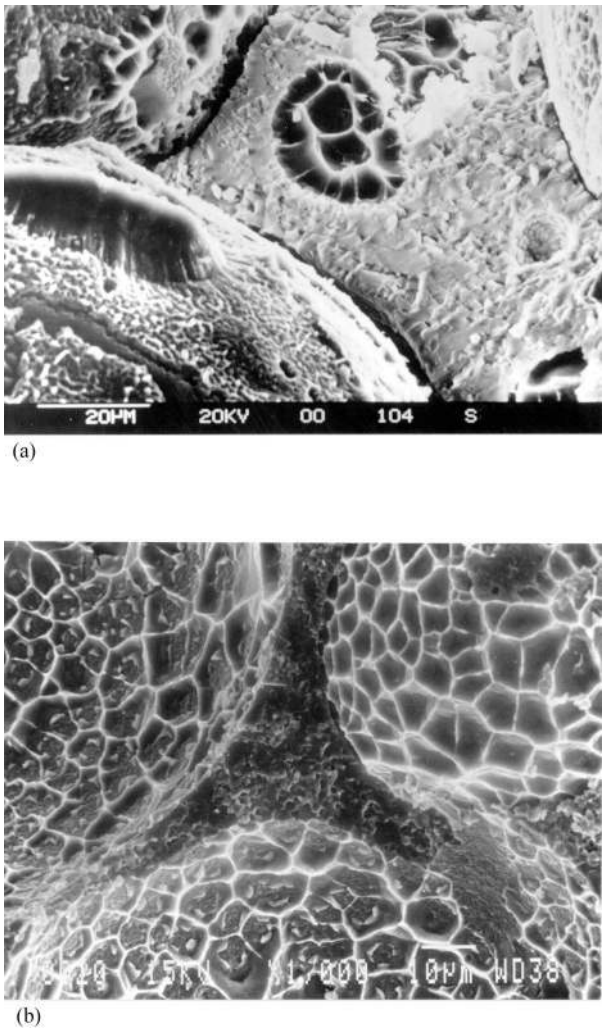

Fig. 7. Fracture surface of composite prepared from POR-AL25 foam under (a) the initial processing conditions (I) showing interfacial debonding and (b) the modified processing conditions (II) showing sound interfacial bond in which ductile failure of the aluminium corresponds to ridges of aluminium residue on the ceramic.

ductile deformation of an aluminium window connection is observed. It is surrounded by a ceramic fracture surface. In the upper and lower left are aluminium surfaces which, apart from the ductile 'window fractures' replicate the sintered ceramic surface of the cell walls. The gap of about 3 μm between the aluminium ball and the ceramic wall may have originated during solidification and cooling or been enhanced by fracture but the ceramic wall is free from aluminium attachment apart from isolated nodules of about 1 μm. This indicates that little or no interfacial bonding was formed during infiltration and solidification.

The observations of the fracture surface of the sample prepared by the modified process are quite different as shown in Fig. 7b. This fractograph was mirrored by an identical image taken from the counter-surface so that similar aluminium ball pull-outs were observed on

the metal side of the fracture surfaces leaving a network pattern both on the aluminium balls and the ceramic walls. Fig. 7b shows the dimple-like fracture surface of the residual aluminium phase on the ceramic cell wall (upper left and lower centre). The gap between the aluminium and ceramic observed in Fig. 7a was not seen. The aluminium fracture face is also seen in Fig. 7b (upper right). The fracture surface of aluminium no longer provides a replica of the ceramic surface. Extensive ductile deformation has occurred. Aluminium residue adheres to the ceramic wall after breaking, leaving a uniform grid-like fracture on the aluminium side and uniform cells on the ceramic side. Cracking of the ceramic was also observed. The examination of the fractured ceramic strut shows low porosity. For this sample, the connectivity of the aluminium phase, as shown in Fig. 5, is the lowest and should be compared with Fig. 2a and b, while the connectivity of the alumina phase is the highest.

3.3. The elastic modulus and electrical resistivity of the composites

The measured elastic moduli of the composites are plotted in Fig. 8. The moduli of DURALCAN Al-MMC, Al_2O_3-particle reinforced 6061 Al composites (T6 condition) which have a homogeneous microstructure, are also shown for comparison [24]. As expected, the composites prepared in this work possess higher modulus than the conventional composites at a given volume fraction and this results from the increased connectivity of the ceramic phase.

For the purpose of comparison, Fig. 8 also contains theoretical predictions frequently used for two-phase composite properties. The volumetric rule of mixtures is given by curve A:

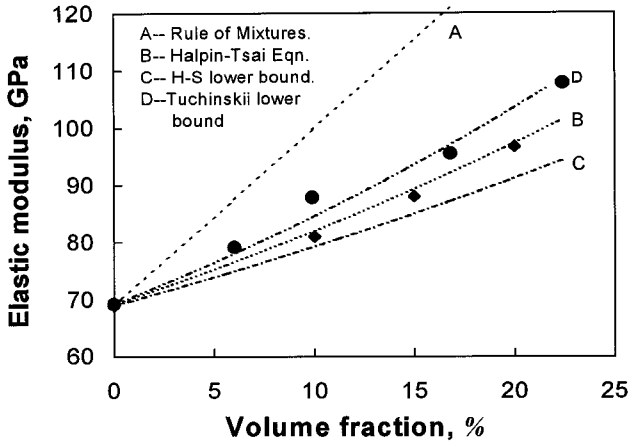

Fig. 8. The measured elastic modulus of the composites (●) and the Duralcan Al-MMC (T6) (◆)[24] compared with theoretical predications by rule of mixtures (A), Halpin–Tsai equation (B) [25], Hashin–Shtrikman equation (C) [24] and Tuchinskii equation (D) [26].

$$E_c = E_m V_m + E_r V_r, \tag{2}$$

where E is the elastic modulus, V the volume fraction and the subscripts c, m and r refer to the composite, matrix and reinforcement, respectively. The values of E_m and E_r are taken as 70 and 380 GPa, respectively.

Curve B is the Halpin–Tsai equation which is a modified rule of mixtures for discontinuous reinforcement [25]:

$$E_c = \frac{E_m(1 + 2sqV_r)}{1 - qV_r}, \tag{3}$$

where

$$q = \frac{(E_r/E_m) - 1}{(E_r/E_m) + 2}, \tag{4}$$

and s is the particle aspect ratio, here, $s = 1$.

Curve C is the Hashin–Shtrikman lower bound [24]:

$$E_c = \frac{E_m[E_m V_m + E_r(V_r + 1)]}{E_r V_m + E_m(V_r + 1)}, \tag{5}$$

besides these theoretical predications, a specific model for the structures consisting of two interpenetrating networks was developed by Tuchinskii [26] which gives the following expression (lower bound) and is represented by curve D:

$$E_c = E_m(1 - t)^2 + E_r t^2 + \frac{2E_r t(1 - t)}{t + (E_r/E_m)(1 - t)}, \tag{6}$$

where the parameter t is related to the volume fraction V_r by

$$V_r = (3 - 2t)t^2. \tag{7}$$

It can be seen that the measured moduli are higher than the predictions (B) and (C) but still lower than the maximum theoretical values as given by the rule of mixtures. It can also be seen that the Halpin–Tsai equation gives a good representation of the experimental results of the composite with a homogeneous microstructure but under-estimates the elastic modulus of the composite produced in the present work. However, the Tuchinskii model does give a good representation of the experimental results for the composite produced in the present work.

Fig. 9 shows the electrical resistivity of the composites as a function of the ceramic volume fraction. In the volume fraction range of 0–20%, the increase of the ceramic volume fraction has negligible influence on the resistivity. Only when the window to cell diameter ratio (k) in the preform is smaller (< 0.17) and hence the aluminium phase has low connectivity does the electrical resistivity increase significantly.

Theoretical predications of the electrical resisitivity (ρ) of multiphase composites are also shown in Fig. 9. The simplest rule of mixture for a parallel array which yields the maximum conductivity of a composite system is given by curve (a) and the equation is written in the notation of this paper:

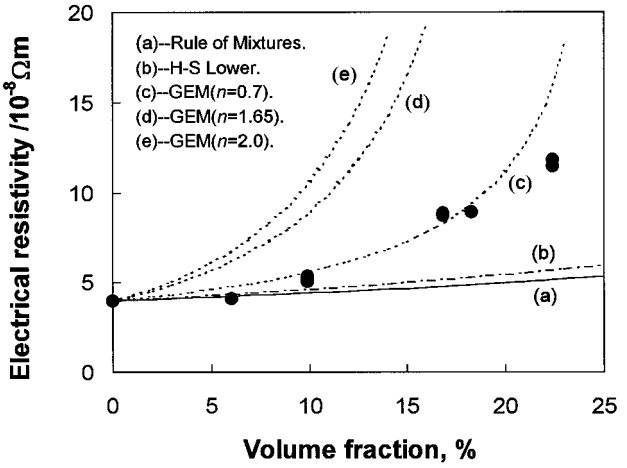

Fig. 9. The measured electrical resistivity of the composites (●) compared with theoretical predications by rule of mixtures (a), Hashin–Shtrikman equation (b) [27] and General Effective Media equation with various n values (c, d, and e) [28].

$$\frac{1}{\rho_c}=\frac{1}{\rho_m}V_m+\frac{1}{\rho_r}V_r, \tag{8}$$

curve (b) is Hashin–Shtrikman lower bound (H–S lower) [27]:

$$\frac{1}{\rho_c}=\frac{1}{\rho_m}+\frac{V_r}{\rho_r\rho_m/(\rho_m-\rho_r)+\rho_m V_m/3}. \tag{9}$$

The general effective media (GEM) equation introduced by McLachlan et al. [28] fits electrical resistivity as a function of volume fraction data for a range of binary composites. For systems consisting of highly conductive aluminium phase ($\rho_m = 4.0\times10^{-8}$ Ωm) and insulating alumina phase ($\rho_r > 10^{14}$ Ωm), the equation can be written as:

$$\frac{1}{\rho_c}=\frac{1}{\rho_m}\left(1-\frac{V_r}{V_r^c}\right)^n, \tag{10}$$

where, $V_r^c$is the critical volume fraction (percolation threshold) of the ceramic phase. This can be taken as 0.26 for the model of the ceramic foam used in the present work which is based on a FCC cell structure. The value of the exponent n for composites is most often found to lie in the range 1.65–2.0 however, it is sometimes found to be below this range and often has a value well in excess of 2.0 [28]. In Fig. 9, curves (c), (d) and (e) are GEM predications with $n = 0.7$, 1.65 and 2.0, respectively.

From Fig. 9, it can be seen that, as expected, the rule of mixture gives the lowest predicted values of the resistivity while the Hashin–Shtrikman equation gives a slightly higher prediction but still below the experimental data, particularly, when the volume fraction exceeds 10%. As to the GEM predictions, the 'universality' range of 1.65–2.0 for exponent n does not fit our experimental results and the best fit occurs when $n =$ 0.7. Even at this value, the equation still over-estimates the resistivities of the composites when the volume fraction exceeds 20%. This indicates that the composites prepared in the present study do have a higher electrical conductivity than that of the majority of the composite systems for which this equation has been tested.

4. Conclusions

Alumina-aluminium composites with interpenetrating microstructures can be fabricated by infiltrating an alumina preform which had the structure of a reticulated ceramic foam. The microstructure of the preform fitted an established relationship between window diameter/cell diameter ratio (k) and void volume fraction (V_p).

Ceramic foams with low k values can be infiltrated fully but on cooling below the solidus, interfacial debonding took place. This was overcome by extending the dwell time of solidification pressure in the temperature range between the solidus and the liquidus. The improvement was observed by microscopy and confirmed by fractography which showed ductile aluminium fracture with aluminium residue on the ceramic cell walls. High k foams which had high V_p retained sound interfacial bonding.

For a given ceramic volume fraction, these composites possess higher elastic modulus than those of conventional MMCs with homogeneous reinforcement distribution. The increase of electrical resistivity is negligible in the lower ($< 20\%$) volume fraction range.

Acknowledgements

The authors are grateful to EPSRC for the financial support of this work under Grant No. GR/L80553. Thanks are given to Linda Orkney and Dr Bryan Roebuck of the National Physical Laboratory, Teddington, UK for their assistance in the modulus and electrical resistivity measurements.

References

[1] D.R. Clarke, J. Am. Ceram. Soc. 75 (1992) 739.
[2] R.E. Newnham, D.P. Skinner, L.E. Cross, Mater. Res. Bull. 13 (1978) 525.
[3] Z. Fan, P. Taakiropoulos, A.P. Miodownik, Mat. Sci. Tech. 8 (1992) 922.
[4] Z. Fan, A.P. Miodownik, Acta Metall. Mater. 41 (1993) 2403–2415.
[5] Z. Fan, Phil. Mag. 73 (1996) 1663.
[6] O. Sigmund, Mech. Mater. 20 (1995) 352.
[7] L.H. Sperling, V. Mishra, Polymer for Advanced Technologies 7 (1996) 197.

[8] J.L. Yu, Y.M. Liu, B.Z. Jiang, Polymer composites 15 (1994) 488.
[9] F.F. Lange, B.V. Velamakanni, A.G. Evans, J. Am. Ceram. Soc. 73 (1990) 388.
[10] R.M. de Souza, H.N. Yoshmura, C. Xavier, H. Goldenstein, Key Eng. Mat. 127–131 (1997) 439.
[11] M. Hoffman, B. Fiedler, T. Emmel, H. Prielipp, N. Claussen, D. Gross, J. Rödel, Acta Mater. 45 (1997) 3609.
[12] S. Skirl, M. Hoffman, K. Bowman, S. Wiederhorn, J. Rödel, Acta Mater. 46 (1998) 2493.
[13] G.S. Daehn, B. Starck, L. Xu, K.F. Elfishawy, J. Ringnalda, H.L. Fraser, Acta Mater. 44 (1996) 249.
[14] H. Prielipp, M. Knechtel, N. Claussen, S.K. Streiffer, H. Müllejans, M. Rühle, J. Rödel, Mat. Sci. Eng., 1995, A197, 19–30.-261.
[15] J. Bruhn, S. Schicker, D.E. Garcia, R. Janssen, F. Wagner, N. Claussen, Key Eng. Mat. 127–131 (1997) 73.
[16] R.E. Loehman, K.G. Ewsuk, A.P. Tomsia, J. Am. Ceram. Soc. 79 (1996) 27.
[17] R.E. Loehman, K.G. Ewsuk, W.F. Fahrenholtz, B.B. Lakshman, Key Eng. Mat. 127–131 (1997) 431.
[18] J. Saggio-Woyansky, C.E. Scott, W.P. Minnear, Am. Ceram. Soc. Bull. 71 (1992) 1674.
[19] P. Sepulveda, Am. Ceram. Soc. Bull. 76 (1997) 61.
[20] H.X. Peng, Z. Fan, J.R.G. Evans, J. Euro. Ceram. Soc. 20 (2000) 807–813.
[21] D.K. Balch, T.J. Fitzgerald, V.J. Michaud, A. Mortensen, Y.-L. Shen, S. Suresh, Metall. Mat. Trans. A. 27A (1996) 3700–3717.
[22] H.X. Peng, Z. Fan, J.R.G. Evans, Ceram. Int. 26 (2000) 887–895.
[23] R. Kolhe, C.Y. Hui, E. Ustundag, S.L. Sass, Acta Mater. 44 (1996) 279–287.
[24] I.A. Ibrahim, F.A. Mohamed, E.J. Lavernia, J. Mat. Sci. 26 (1991) 1137–1156.
[25] D.J. Lloyd, Inter. Mat. Reviews 39 (1994) 1–24.
[26] L.I. Tuchinskii, Soviet Powder Metall. Metal Ceramics 85 (1983) 588–595.
[27] Z. Hashin, S. Shtrikman, J. Appl. Phys. 33 (1962) 3125–3131.
[28] D.S. McLachlan, M. Blaszkiewicz, R.E. Newnham, J. Am. Ceram. Soc. 73 (1990) 2187–2203.